

Language-Conditioned Offline RL for Multi-Robot Navigation

Steven Morad

Dept. of Computer Science and Technology
University of Cambridge
United Kingdom
sm2558@cst.cam.ac.uk

Ajay Shankar

Dept. of Computer Science and Technology
University of Cambridge
United Kingdom
as3233@cst.cam.ac.uk

Jan Blumenkamp

Dept. of Computer Science and Technology
University of Cambridge
United Kingdom
jb2270@cst.cam.ac.uk

Amanda Prorok

Dept. of Computer Science and Technology
University of Cambridge
United Kingdom
asp45@cst.cam.ac.uk

Abstract: We present a method for developing navigation policies for multi-robot teams that interpret and follow natural language instructions. We condition these policies on embeddings from pretrained Large Language Models (LLMs), and train them via offline reinforcement learning with as little as 20 minutes of randomly-collected data. Experiments on a team of five real robots show that these policies generalize well to unseen commands, indicating an understanding of the LLM latent space. Our method requires no simulators or environment models, and produces low-latency control policies that can be deployed directly to real robots without finetuning. We provide videos of our experiments at <https://sites.google.com/view/llm-marl>.

Keywords: Multi-Robot, Multi-Agent Reinforcement Learning, Large Language Models

1 Introduction

Natural language provides a rich and intuitive interface to describe robot tasks. For instance, commands such as “navigate to the left corner” or “pick up the can” lend themselves as more powerful and flexible alternatives to specifying (x, y) coordinates or joint configurations. Using language descriptions to specify outcomes, particularly when interfacing with a team of robots, is thus a more natural choice, and one that does not require specially-trained operators.

Recent work on commanding robots with natural language tend to utilize large pretrained transformers [1] known as LLMs [2, 3, 4] or Large Multimodal Models (LMMs) [5] for both language processing and control. Often, the transformer receives a task and observation, and produces either an action or a sequence of actions to complete the task [6, 7, 8, 9]. The latter case reduces to open-loop control, which cannot adapt to uncertainty, while the former is limited by the high latency of these models, typically measured in seconds or hundreds of milliseconds, precluding them from dynamic scenarios. These drawbacks are especially restricting in *multi-agent* scenarios, where agents need closed-loop control to react and replan quickly based on the observed behavior of other robots [10, 11, 12]. Developing multi-agent policies that can capitalize on the power of LLMs while retaining fast, reactive, and emergent team behavior is therefore a hard problem.

In this work, we present a method that maps high-level natural language commands directly to control outputs for a multi-robot system. First, we project natural language instructions into a latent space using a pretrained LLM, and then condition control policies on these latent embeddings. By

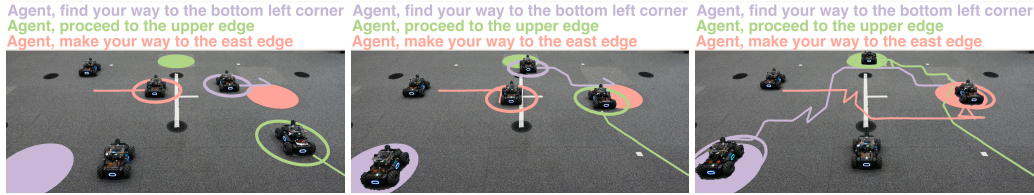


Figure 1: Our learned policies demonstrate emergent path deconfliction while following natural-language tasks. Agents, tasks, and goals are color-coordinated. Each agent (hollow disk) receives a natural language task (top), and must navigate to the goal (filled disk, rendered for visualisation only), leaving behind a colored trail. All five agents are in motion, but we highlight tasks and goals for three they execute a three-way yield. (Left) The red, purple, and green agents block each other from reaching their respective goals. (Middle) Green moves towards its goal and purple yields to green by moving north, and red yields to purple by remaining stationary. (Right) After green completes its task, purple and red complete their tasks.

factoring the LLM outside of the control loop, we achieve low-latency (< 2 ms) realtime control. Our approach then generates a large multi-agent dataset using random real-world actions of a single robot. We train our task-conditioned policies on this real-world dataset using *offline* Reinforcement Learning (RL). Because we train our policies on real data, we can deploy our policies back into the real world without any finetuning.

Contributions We claim the following key contributions:

- an architecture that enables low-latency multi-agent control through natural language;
- a method to generate large amounts of multi-agent training data from a single robot;
- findings that a one-line change to Q-learning improves offline training stability;
- evidence that our policies can generalize to unseen commands, solely through value estimation; and,
- the first demonstration of offline multi-agent RL on robots in the real-world.

2 Related Work

LMMs such as GPT [2] and LLMs such as LLaMa or Mistral [3, 4] demonstrate strong emergent reasoning capabilities, mapping a series of input tokens to output tokens using a transformer architecture [1]. Given their similarities, we refer to both LLMs and LMMs as LLMs moving forward. LLMs often output tokens in the form of text, however, recent work has integrated them into robotic applications due to their powerful reasoning capabilities. For instance, PaLM-E [6] ingests image and text tokens and outputs text describing a list of steps to follow. Prior work demonstrates zero-shot navigation to visual targets by outputting text tokens that map to physical actions [7]. In [9], the authors chain an LLM to a visual foundation model for visual navigation. Going one step further, the method in [8] outputs tokens that correspond to actions, rather than text tokens. Certain works learn policies using imitation learning [13] or value functions [14] for textual action primitives output by an LLM. LLMs are often slow to execute, and these works are often not explicit about the latency between perception and action. For example, the smallest LLaMa-v2 model has roughly 100x fewer parameters than PaLM-E model used in [6]. After 2-bit quantization and other efficiency tricks, LLaMa-v2 produces less than two tokens per second on an NVidia Jetson AGX Orin [15]. Given that outputs often consist of multiple tokens, today’s hardware precludes them from low-latency and reactive control tasks necessary in multi-robot systems.

The use of LLMs in multi-robot systems is still in its infancy, and similar to single-robot settings, relies on mapping text-tokens to plans or actions. Thus, they inherit the latency bottleneck of LLMs, compounded by generating tokens for an increased number of robots. Most prior work operates in simulation, with few papers demonstrating real-world implementations [16]. In [17, 18, 19], individual agents converse in simulation to form a multi-agent system, with the agents eventually

outputting text tokens for control. LLMs resolve deadlocks in a simulated multi-robot navigation task, by outputting text tokens that correspond to agent directions [20]. Another approach allocates tasks to agents using an LLM [16]. Like with single-agent LLM control, these approaches are generally not suitable for realtime control.

3 Background

Sentence Similarity LLMs We are interested in a class of LLMs known as sentence similarity or feature extraction LLMs [21, 22, 23]. An LLM maps n input tokens map to n latent representations at each transformer layer. The final layer predicts a token given n latent representations. Rather than mapping to a token index, feature extraction LLMs pool over the final latent representation to return an embedding that summarizes the input text. These models are trained to have meaningful latent representations, such as semantic similarity corresponding to cosine similarity or Euclidean distance in the latent space. For example, the latent representation of “quick brown fox” would be closer to “fast maroon badger” than “machine learning”.

Reinforcement Learning We refer the reader to [24] for a proper treatment of reinforcement learning. Reinforcement learning aims to learn a policy π to maximize cumulative rewards in a Markov Decision Process (MDP) $\langle S, A, R, T, \gamma \rangle$. The agent selects actions $a \sim \pi(s)$ to transition to new states $T(s'|s, a)$ and receive rewards $r = R(s, a, s')$, with the goal of maximizing $\mathbb{E}_\pi [\sum_{t=0}^{\infty} \gamma^t R(s, a, s')]$. For value-based policies, we will often attempt to learn the value of states s using either a value function $V(s_0) = \mathbb{E}_\pi [\sum_{t=0}^{\infty} \gamma^t R(s, a, s')]$, or a Q function $Q(s_0, a_0) = R(s_0, a_0, s_1) + \mathbb{E}_\pi [\sum_{t=1}^{\infty} \gamma^t R(s, a, s')]$. We then follow a policy that maximizes V or Q , such as the greedy policy $\pi(s) = \operatorname{argmax}_{a \in A} Q(s, a)$.

Multi-Agent RL We direct the reader to [25] for a review of Multi-Agent Reinforcement Learning (MARL). It has a number of formulations, depending on the structure of the reward functions. We extend the MDP above to a Decentralized MDP with factorized rewards, defined as $\langle S, \mathcal{A}, T, \mathcal{R}, \mathcal{O}, \Omega, \gamma \rangle$. Each agent i has its own action space, reward function, and observation function: $\mathcal{A} = \{A_i\}_{i=1}^n, \mathcal{R} = \{R_i\}_{i=1}^n, \mathcal{O} = \{O_i\}_{i=1}^n$. The state $s \in S$ is a function of local observations $s = f(o_1, \dots, o_n)$, where each observation $o_i \in \Omega$ is found via $o_i \sim O_i(s)$. The state transition function is $T : S \times \mathcal{A} \mapsto S$, and the reward function $R_i(s, a, s')$ is defined on the states. There are a variety of MARL algorithms that focus on multi-agent credit assignment, such as MADDPG [26], QMix [27], and COMA [28]. Given our factorized reward function, we choose to learn independent policies using algorithms like Independent Proximal Policy Optimization (IPPO) [29] or Independent Q-Learning (IQL) [30]. Additionally, [31] proposes a softmax-regularized form of the Q-learning objective that provides better results in MARL.

Offline RL Offline RL learns a policy from existing data, which is especially useful in robotics, where simulators can be inaccurate and data collection can be costly. Unlike imitation learning which requires expert data, offline RL can learn policies from *completely random data*. In offline RL, we no longer have direct access to the MDP or DecMDP. Instead, a behavior policy π_β collects transition tuples $\langle s, a, r, s' \rangle$ (or $\langle o_i, a_i, r_i, o'_i \rangle$ in the multi-agent case). With fixed datasets, standard value functions tend to *overextrapolate* – incorrectly estimating values for out-of-distribution transitions, which propagate via bootstrapping. Solutions like Conservative Q-Learning (CQL) regularize value estimates to prevent positive overextrapolation [32, 33, 34], while others constrain the learned policy to be close to the data collection policy π_β [35, 36]. There is little work combining MARL with offline RL, likely because both offline RL and MARL are difficult to solve individually. Prior work proposes counterfactual offline multi-agent Q-learning based on CQL [34, 32] and Implicit Constraint Q-Learning (ICQ), which uses soft Q-learning to prevent overextrapolation [37].

Task-Conditioned Policies There are a number of names for task-conditioned reinforcement learning. It is sometimes called goal-conditioned RL, multi-task RL, or universal value function approximation [38, 39, 40]. Although formulated in different ways, the key difference

between these and ‘standard’ RL is the introduction of a *task* or *goal* $g \in G$ into the reward and value functions, as well as the policy: $\langle R(s, a, s'), V(s), Q(s, a), \pi(s) \rangle$ becomes $\langle R(s, a, s'|g), V(s|g), Q(s, a|g), \pi(s|g) \rangle$. Thus, instead of learning a value function and policy for a specific task, we learn one that can generalize over a task space G .

4 Approach

Our objective is to train multi-agent policies to follow natural language navigation tasks. Our approach consists of two distinct parts, *creating the dataset* and *training the model*. To generate the dataset, we first collect real-world data using a *single robot*. Then, we generate a large quantity of natural language tasks. We sample real-world data and tasks independently, combining them to form a large multi-agent dataset. Finally, we train a policy on the multi-agent dataset using offline RL.

4.1 Dataset Creation and Augmentation

We use the DJI RoboMaster, a four-wheel mecanum-drive holonomic robot, for our experiments [41]. We collect a dataset \mathcal{D} by recording $\langle s, a, s' \rangle$ tuples from a single robot as it uniformly samples actions from the action space ($a \sim \mathcal{U}(A)$). We record one tuple per second, resulting in a total of 5400 tuples spanning 90 minutes of data collection. The state space S consists of two-dimensional position and velocity vectors, while the action space A consists of 9 discrete actions, corresponding to eight direction vectors (at 0.3 m/s each), plus an action that corresponds to zero velocity.

Generating Task Embeddings Each task $g \in G$ is a natural language task, such as `Agent, the south west corner is your target`. We encode each task into a latent embedding $z = \phi(g)$ using a feature extraction LLM. Each agent in the multi-agent system independently receives tasks, and the tasks differ between agents. For example, one robot might receive the task `Agent, the south west corner is your target`, while another might receive `Agent, navigate to the left edge`. We split our tasks and embeddings into a set of *train tasks* and *test tasks*. We use 396 tasks for the train set and eight tasks for the test set (Appendix D). Each item in our test set is a *never before seen* command, enabling us to gauge our model’s generalization capabilities.

Combinatorial Multi-Agent Augmentation Rather than collect a multi-agent dataset, we choose to collect a single agent dataset because it can be exploited to create a large multi-agent dataset in certain scenarios. To turn our single agent dataset into a multi-agent one, we combine single agent transitions into a multi-agent transition

$$s = \langle s_i, s_j, s_k, \dots \rangle, a = \langle a_i, a_j, a_k, \dots \rangle, s' = \langle s'_i, s'_j, s'_k, \dots \rangle, \quad i, j, k \in \mathcal{U}(|\mathcal{D}|). \quad (1)$$

This process creates a large amount of multi-agent data from a small amount of single agent data. For example, from our 5400 single agent transitions, we can create a three agent dataset with $\text{Permute}(5400, 5) \approx 10^{18}$ transitions. Given our 396 task embeddings and five agents, we can generate $\text{Permute}(396, 5) \approx 10^{12}$ multi-agent task configurations. The product of these two sets results in 10^{30} possible task-transition configurations. Given our sample rate, this would equate to collecting data for a duration 10^{12} times the age of the universe – for this reason, we never physically materialize the multi-agent dataset. Rather, we construct these multi-agent transitions on the fly by uniformly sampling transitions with replacement $\langle s_i, a_i, s'_i \rangle \sim \mathcal{U}(\mathcal{D})$ and tasks without replacement $g_j \sim \mathcal{U}(G)$.

Reward and Termination Functions For each agent i , we create a task-conditioned reward function R_i and episode termination function D_i . We compute the reward and termination conditions across various tasks g_j and corresponding goal coordinates r_j as

$$R_i(s, a, s', g_j) = (\|p'_i - r_j\|_2 - \|p_i - r_j\|_2)(1 + v'_i + v_i) - c(p'_i, s) \quad (2)$$

$$D_i(s, a, s', g_j) = c(p'_i, s), \quad (3)$$

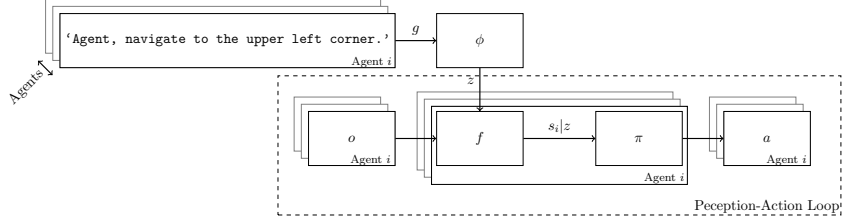


Figure 2: Our proposed multi-robot model architecture. Each agent receives a different natural language task and a local observation. We summarize each natural language task g_i into a latent representation z_i , using an LLM ϕ . The function f is a graph neural network that encodes local observations o_1, o_2, \dots and task embeddings z_1, z_2, \dots into a task-dependent state representation $s_i|z$ for each agent i . We learn a local policy π conditioned on the state-task representation. Functions π, f are learned entirely from a fixed dataset using offline RL. Because we compute z_i only once per task, the LLM is not part of the perception-action loop, allowing the policy to act quickly.

where p_i, v_i corresponds to the position and velocity portions of the state for agent i . The function c computes collisions between individual agents as well as with the walls. The first term in the reward function provides a reward for moving closer to the goal, scaled by a velocity to create smoother movement. The second reward term penalizes collisions. This reward function ensures that each agent reaches its goal quickly while avoiding collisions, similar to prior work [42].

4.2 Training Objectives

As stated in Section 3, there are a number of offline RL algorithms, however, the majority are designed for single agent setups. Furthermore, most focus on continuous action spaces and thus utilize KL divergence, causing a divide-by-zero error when considering the greedy policy. Instead, we reformulate Q-learning through the lens of *Expected SARSA*, a relatively understudied [43] form of value approximation from the Sutton and Barto textbook [24]. In the following subsection, we show how Expected SARSA subsumes approaches like Max Q-learning, softmax-regularized Q-learning [31], and Mean Q-learning [44]. Furthermore, we can implement Expected SARSA on top of Q-learning by changing a single line of code (Appendix A).

Extending Expected SARSA to Offline Datasets Expected SARSA results in lower variance updates than standard Q-learning [24, 6.6], which is useful in offline learning scenarios where a single bad update can trigger instabilities that result in runaway overextrapolation of Q values [24, 35, 6.6]. Expected SARSA generally results in safer, albeit less optimal policies than Q-learning, as demonstrated in the famous cliffwalker experiment [24, 43, 6.5] (Appendix A). This is especially useful in robotics, where safer policies may be preferred over optimal policies. More formally, Expected SARSA learns a policy-weighted value approximation

$$Q_\pi(s, a) = R(s, a, s') + \gamma \sum_{a' \in A} \pi(a'|s') Q_\pi(s', a'). \quad (4)$$

However, Expected SARSA is not designed for offline RL. Normally, a stochastic exploratory policy is slowly annealed into an optimal deterministic Max Q policy. In offline RL, we cannot access the MDP and thus cannot explore. Therefore, it is unclear what to use for π in Eq. (4). If we plug in the standard greedy policy, Expected SARSA decomposes into the standard Max Q-learning objective

$$Q_*(s, a) = R(s, a, s') + \gamma \sum_{a' \in A} \delta_{\text{argmax}_{a' \in A} Q_*(s', a')} Q_*(s', a') \quad (5)$$

$$= R(s, a, s') + \gamma \max_{a' \in A} Q_*(s', a') \quad (6)$$

where δ is the Kronecker delta (indicator) function. As discussed in Section 3, Max Q-learning struggles in purely offline scenarios. On the other hand, using the collection policy $\pi = \pi_\beta$ in the objective could prevent overextrapolation at the expense of less optimal behavior. Given that our

dataset was collected by sampling actions from a uniform distribution $\pi_\beta = \mathcal{U}(|A|)$, substituting π_β into Expected SARSA results in a Mean Q-learning objective similar to [44]

$$Q_\beta(s, a) = R(s, a, s') + \gamma \sum_{a' \in A} \mathcal{U}(|A|) Q_\beta(s', a') = R(s, a, s') + \gamma \sum_{a' \in A} \frac{1}{|A|} Q_\beta(s', a') \quad (7)$$

$$= R(s, a, s') + \gamma \operatorname{mean}_{a' \in A} Q_\beta(s', a'). \quad (8)$$

We can also parameterize the space of policies between π and π_β using the softmax operator. This corresponds to optimizing the softmax-regularized MARL objective [31], and also resembles the ICQ objective [37]

$$Q_\sigma(s, a) = R(s, a, s') + \gamma \left[\sum_{a' \in A} \left(\frac{e^{Q_\sigma(s', a')/\tau}}{\sum_{\alpha' \in A} e^{Q_\sigma(s', \alpha')/\tau}} \right) Q_\sigma(s', a') \right] \quad (9)$$

where τ is a temperature hyperparameter. As $\tau \rightarrow 0$, Soft Q becomes Max Q, and as $\tau \rightarrow \infty$, Soft Q becomes Mean Q. We investigate all of these objectives in our experiments.

Model Architecture Given that we can factorize rewards in the navigation scenario, we opt for a variant of Expected SARSA in the style of IQL with shared observations [30]. Each agent approximates their own embedding of the global state $s_1, s_2, \dots, s_m \in S$, given a set of local observations $o_1, o_2, \dots, o_n \in O$ using a function f (Fig. 2). Although it is conceptually simpler to model $f : O^n \mapsto S, \pi(s_i, z_i)$, we find that conditioning the state s_i on z performs better in practice: $f : O^n \times Z^n \mapsto S, \pi(s_i|z)$. This formulation enables agents to tailor their state representation based on the assigned tasks. Given n agents, we model f using a graph neural network over a fully-connected graph. We compute each s_i using a pairwise nonlinear function over each robot’s task and sensor information

$$s_i = \frac{1}{n} \sum_{1 \leq j \leq n} B(o_i || z_i || o_j || z_j), \quad B(x) = \sigma[\text{LN}(Wx + b)], \quad (10)$$

where $||$ represents concatenation B and represents a block with a learnable parameters W, b , layer normalization LN [45], and leaky ReLU activation σ [46]. Each agent predicts their Q value $Q(s_i|z, a_i)$ independently, following one of the previous Q-learning methods from Section 4.2. Our Q function consists of two consecutive blocks B , followed by a dueling Q linear layer [47]. We use the clipped double Q trick [48] to further increase training stability.

5 Experiments and Discussion

Our experiments aim to answer four key questions: (1) Is it possible to generalize to an LLM latent space? (2) Which loss function should we use to train our policy? (3) How much data must we collect to train a suitable policy? (4) How does our policy perform on real robots?

LLM Latent Space Analysis In our first experiment, we quantify how likely a policy is to generalize to the LLM latent space. Recall that we map a natural language goal to a latent embedding using an LLM $z = \phi(g)$. Now, we attempt to learn a decoder ψ that maps the latent goal embedding to an alternative representation of the goal $\bar{g} = \psi(z)$. If we can correctly predict \bar{g} for a never-before-seen g , we say that the decoder has *generalized* to the latent space. To this end, we train an MLP decoder to regress a 2D goal coordinate. For example, the embeddings of ‘navigate to the left edge’ and ‘the west edge is your target’ should both decode to $\bar{g} = (-k, 0)$ for some given k . If our learned decoder ψ , never having seen the phrases ‘go to the’ or ‘north east corner’, can correctly decode ‘go to the north east corner’ to $\bar{g} = (k, k)$, then we say that our decoder has generalized to the LLM latent space.

We compare several LLMs and plot the mean position test error in Fig. 3, utilizing the train and test split from Section 4.1. We find that certain LLMs are not suitable for our purposes (e.g., MiniLM has an error of nearly 1 m). The GTE-Base LLM [22] is a good tradeoff between latent size and performance, with a mean error of 7 cm across never-before-seen tasks. Therefore, we use the GTE-Base LLM in all further experiments.



Figure 3: (Left) A comparison of LLMs [49, 50, 51, 52, 21, 22, 4, 53] used for feature extraction. Our decoder only generalizes to certain LLM latent spaces (note the log scale y-axis). (Right) Control latency (observation to action) for different team sizes, tested on a 2020 MacBook Air CPU. Our policies map perception to action much faster than those with an LLM in the perception-action loop, which can often take seconds to produce each action.

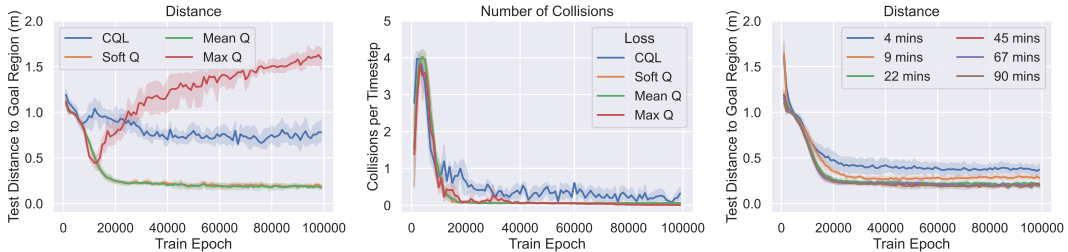


Figure 4: (Left Two) We compare the best CQL and Soft Q variants to Max Q and Mean Q objectives. Soft Q and Mean Q perform best. (Rightmost) We experiment with how much data collection is necessary to train a sufficient policy, using the Mean Q objective.

5.1 Simulation Experiments

Although our approach does not require a simulator to learn a policy, they can be helpful for analysis. To this end, we learn a single-agent state transition model from our dataset $s'_i = T_i(s_i, a_i)$, where T_i is approximated using a deep neural network. We create a multi-robot simulator via $T(s, a) = \{T_i(s_i, a_i)\}_{i=1}^n$. This model is not perfect – for example, we can detect collisions between agents but cannot model them. That said, it still allows us to probe various objective functions.

Objective Function Analysis In Section 4.2, we discuss a number of optimization objectives. Using our simulator, we compare the resulting policies trained using each of these objectives. We report metrics on the *test tasks* which were not seen during training (Section 4.1). In Appendix B.1, we explore various CQL regularization strengths and Soft Q temperatures for an Expected SARSA Soft Q objective. We compare the best performing CQL and Soft Q variants to the Max Q and Mean Q weightings in Fig. 4, along with perception to action latency. We report the mean distance to the goal over an episode, as well as the number of collisions.

Max Q begins to overextrapolate around 15k epochs, similar to findings in prior work [35, 54]. CQL’s regularization improves upon the Max Q performance. Both Mean Q and Soft Q perform comparably, outperforming both CQL and Max Q with respect to distance and number of collisions. The strong performance of Mean Q suggests that strong regularization towards the dataset collection policy π_β is necessary, even though the regularization reduces optimality. This echoes findings from [44], where maximizing the Mean Q Monte Carlo return can outperform CQL. Both Mean Q and Soft Q objectives have nonzero weight over all state-action values. For every state, they always consider the in-distribution action collected during training, which can “ground” the value estimate and further prevent overextrapolation error.

Data Efficiency We investigate how the policy degrades as we reduce the amount of training data available. We subsample our dataset into smaller datasets, and report the results in Fig. 4 right). We find the performance remains nearly the same with as little as 22 minutes of data. Our results also show that we can learn an imperfect yet reasonable policy from just four minutes of real world data.

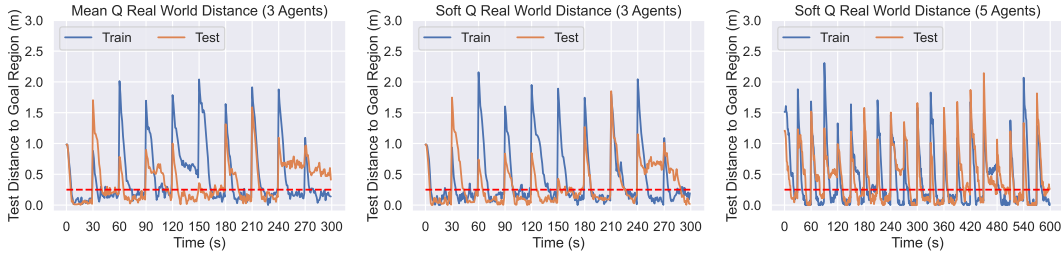


Figure 5: Evaluations from real-world multi-agent navigation tests, where each agent is provided a new task every 30 s. We plot their distance from the goal (averaged over agents) as they navigate. The blue line represents tasks the agent has seen before, while the orange line represents unseen tasks. Our results show that our agents are able to generalize to unseen, out-of-distribution tasks. We consider success as reaching a mean distance < 25 cm (red line) from the goal regions. For three agents, the Mean Q policy solves 9/10 train tasks and 8/10 test tasks while the Soft Q policy solves 10/10 train tasks and 9/10 test tasks. For five agents, the Soft Q policy solves 19/20 train tasks and 18/20 test tasks. See Appendix B for other objectives.

We suspect this is possible for two reasons: (1) Our nearly four hundred tasks correspond to nearly four hundred losses for each transition in our dataset. (2) The way we build our multi-agent dataset allows for a combinatorial number of possible agent configurations (Section 4.1).

5.2 Real World Experiments

Combining offline RL with real-world data should enable us to deploy our policies directly to real robots. In this experiment, we validate that our policies can succeed in the real world without any finetuning. We select the best performing hyperparameters for each loss function in Appendix C.3, and deploy the resulting policies onto either three or five robots. We evaluate each policy twice: once on train tasks, and once on test tasks (Fig. 5, Fig. 1). We consider a task “solved” if the mean distance to the goal region is less than 0.25 m.

In Fig. 5, we find that the policies trained using soft and mean objectives solve most of the train tasks and *generalize* to the never-before-seen tasks in the test set. Additionally, we observe zero collisions in our 40 minutes of 3-agent tests, and two minor scrapes in our 20 minutes of 5-agent tests. Upon further investigation, the scrapes appear related to issues in the motion capture system, as explained in Appendix B.3. Policies trained with CQL and Max Q move the agents to the edge of the boundaries and keep them there, regardless of the objective. These policies likely learn this behavior to avoid collisions between agents, but are unable to learn to navigate to the given goals. Meanwhile, policies trained using the Mean Q and Soft Q objectives reliably navigate agents to their goals.

6 Limitations and Conclusion

Given the complexity of fusing offline RL, LLMs, and MARL for real-world robots, we scoped this work to navigation tasks. Future work could extend our methodology towards larger and more general task-spaces. We were able to use a simple IQL learning algorithm because our navigation task has easily factorable rewards. This factorization also enabled us to utilize single-agent data. For more complex tasks with global rewards, future work could collect multi-agent datasets and train using MADDPG. This would also unlock continuous action spaces, but this would require that both the policy and Q function learn to generalize to the LLM latent space. Our random action selection might not scale to larger state spaces, however Expected SARSA Soft Q should work with any dataset collection policy.

In summary, we proposed a method that maps natural language tasks to multi-robot control outputs, by combining LLMs with offline RL. We generated multi-agent datasets from single agent data, using it to train policies offline. Then, we investigated different learning objectives, and found that

safer policies work better in practice. Our experiments showed that our policies can generalize to never before seen natural language commands, and that we could deploy our policies into the real world without any finetuning.

7 Acknowledgements

We thank Matteo Bettini and Ryan Kortvelesy for their helpful discussions. This work was supported in part by ARL DCIST CRA W911NF-17-2-0181 and European Research Council (ERC) Project 949940 (gAIa).

References

- [1] A. Vaswani, N. Shazeer, N. Parmar, J. Uszkoreit, L. Jones, A. N. Gomez, L. Kaiser, and I. Polosukhin. Attention is All you Need. In *Advances in Neural Information Processing Systems*, volume 30. Curran Associates, Inc., 2017. URL <https://proceedings.neurips.cc/paper/2017/hash/3f5ee243547dee91fbd053c1c4a845aa-Abstract.html>.
- [2] T. B. Brown, B. Mann, N. Ryder, M. Subbiah, J. Kaplan, P. Dhariwal, A. Neelakantan, P. Shyam, G. Sastry, A. Askell, S. Agarwal, A. Herbert-Voss, G. Krueger, T. Henighan, R. Child, A. Ramesh, D. M. Ziegler, J. Wu, C. Winter, C. Hesse, M. Chen, E. Sigler, M. Litwin, S. Gray, B. Chess, J. Clark, C. Berner, S. McCandlish, A. Radford, I. Sutskever, and D. Amodei. Language models are few-shot learners. In *Advances in Neural Information Processing Systems*, volume 2020-Decem, 2020. ISSN: 10495258 .eprint: 2005.14165.
- [3] H. Touvron, L. Martin, K. Stone, P. Albert, A. Almahairi, Y. Babaei, N. Bashlykov, S. Batra, P. Bhargava, S. Bhosale, D. Bikel, L. Blecher, C. C. Ferrer, M. Chen, G. Cucurull, D. Esiobu, J. Fernandes, J. Fu, W. Fu, B. Fuller, C. Gao, V. Goswami, N. Goyal, A. Hartshorn, S. Hosseini, R. Hou, H. Inan, M. Kardas, V. Kerkez, M. Khabsa, I. Kloumann, A. Korenev, P. S. Koura, M.-A. Lachaux, T. Lavril, J. Lee, D. Liskovich, Y. Lu, Y. Mao, X. Martinet, T. Mihaylov, P. Mishra, I. Molybog, Y. Nie, A. Poulton, J. Reizenstein, R. Rungta, K. Saladi, A. Schelten, R. Silva, E. M. Smith, R. Subramanian, X. E. Tan, B. Tang, R. Taylor, A. Williams, J. X. Kuan, P. Xu, Z. Yan, I. Zarov, Y. Zhang, A. Fan, M. Kambadur, S. Narang, A. Rodriguez, R. Stojnic, S. Edunov, and T. Scialom. Llama 2: Open Foundation and Fine-Tuned Chat Models, July 2023. URL <http://arxiv.org/abs/2307.09288>. arXiv:2307.09288 [cs].
- [4] A. Q. Jiang, A. Sablayrolles, A. Mensch, C. Bamford, D. S. Chaplot, D. d. I. Casas, F. Bressand, G. Lengyel, G. Lample, L. Saulnier, L. R. Lavaud, M.-A. Lachaux, P. Stock, T. L. Scao, T. Lavril, T. Wang, T. Lacroix, and W. E. Sayed. Mistral 7B, Oct. 2023. URL <http://arxiv.org/abs/2310.06825>. arXiv:2310.06825 [cs].
- [5] OpenAI, J. Achiam, S. Adler, S. Agarwal, L. Ahmad, I. Akkaya, F. L. Aleman, D. Almeida, J. Altenschmidt, S. Altman, S. Anadkat, R. Avila, I. Babuschkin, S. Balaji, V. Balcom, P. Batrescu, H. Bao, M. Bavarian, J. Belgum, I. Bello, J. Berdine, G. Bernadett-Shapiro, C. Berner, L. Bogdonoff, O. Boiko, M. Boyd, A.-L. Brakman, G. Brockman, T. Brooks, M. Brundage, K. Button, T. Cai, R. Campbell, A. Cann, B. Carey, C. Carlson, R. Carmichael, B. Chan, C. Chang, F. Chantzis, D. Chen, S. Chen, R. Chen, J. Chen, M. Chen, B. Chess, C. Cho, C. Chu, H. W. Chung, D. Cummings, J. Currier, Y. Dai, C. Decareaux, T. Degry, N. Deutsch, D. Deville, A. Dhar, D. Dohan, S. Dowling, S. Dunning, A. Ecoffet, A. Eleti, T. Eloundou, D. Farhi, L. Fedus, N. Felix, S. P. Fishman, J. Forte, I. Fulford, L. Gao, E. Georges, C. Gibson, V. Goel, T. Gogineni, G. Goh, R. Gontijo-Lopes, J. Gordon, M. Grafstein, S. Gray, R. Greene, J. Gross, S. S. Gu, Y. Guo, C. Hallacy, J. Han, J. Harris, Y. He, M. Heaton, J. Heidecke, C. Hesse, A. Hickey, W. Hickey, P. Hoeschele, B. Houghton, K. Hsu, S. Hu, X. Hu, J. Huizinga, S. Jain, S. Jain, J. Jang, A. Jiang, R. Jiang, H. Jin, D. Jin, S. Jomoto, B. Jonn, H. Jun, T. Kaftan, L. Kaiser, A. Kamali, I. Kanitscheider, N. S. Keskar, T. Khan, L. Kilpatrick, J. W. Kim, C. Kim, Y. Kim, J. H. Kirchner, J. Kiros, M. Knight, D. Kokotajlo, L. Kondraciuk, A. Kondrich, A. Konstantinidis, K. Kosic, G. Krueger, V. Kuo, M. Lampe, I. Lan, T. Lee, J. Leike, J. Leung, D. Levy, C. M. Li, R. Lim, M. Lin, S. Lin, M. Litwin, T. Lopez, R. Lowe, P. Lue, A. Makanju, K. Malfacini, S. Manning, T. Markov, Y. Markovski, B. Martin, K. Mayer, A. Mayne, B. McGrew, S. M. McKinney, C. McLeavey, P. McMillan, J. McNeil, D. Medina, A. Mehta, J. Menick, L. Metz, A. Mishchenko, P. Mishkin, V. Monaco, E. Morikawa, D. Mossing, T. Mu, M. Murati, O. Murk, D. Mély, A. Nair, R. Nakano, R. Nayak, A. Neelakantan, R. Ngo, H. Noh, L. Ouyang, C. O’Keefe, J. Pachocki, A. Paino, J. Palermo, A. Pantuliano, G. Parascandolo, J. Parish, E. Parparita, A. Passos, M. Pavlov, A. Peng, A. Perelman, F. d. A. B. Peres, M. Petrov, H. P. d. O. Pinto, Michael, Pokorny, M. Pokrass, V. H. Pong, T. Powell, A. Power, B. Power, E. Proehl, R. Puri, A. Radford, J. Rae, A. Ramesh, C. Raymond, F. Real,

- K. Rimbach, C. Ross, B. Rotsted, H. Roussez, N. Ryder, M. Saltarelli, T. Sanders, S. Santurkar, G. Sastry, H. Schmidt, D. Schnurr, J. Schulman, D. Selsam, K. Sheppard, T. Sherbakov, J. Shieh, S. Shoker, P. Shyam, S. Sidor, E. Sigler, M. Simens, J. Sitkin, K. Slama, I. Sohl, B. Sokolowsky, Y. Song, N. Staudacher, F. P. Such, N. Summers, I. Sutskever, J. Tang, N. Tezak, M. B. Thompson, P. Tillet, A. Tootoonchian, E. Tseng, P. Tuggle, N. Turley, J. Tworek, J. F. C. Uribe, A. Vallone, A. Vijayvergiya, C. Voss, C. Wainwright, J. J. Wang, A. Wang, B. Wang, J. Ward, J. Wei, C. J. Weinmann, A. Welihinda, P. Welinder, J. Weng, L. Weng, M. Wiethoff, D. Willner, C. Winter, S. Wolrich, H. Wong, L. Workman, S. Wu, J. Wu, M. Wu, K. Xiao, T. Xu, S. Yoo, K. Yu, Q. Yuan, W. Zaremba, R. Zellers, C. Zhang, M. Zhang, S. Zhao, T. Zheng, J. Zhuang, W. Zhuk, and B. Zoph. GPT-4 Technical Report, Mar. 2024. URL <http://arxiv.org/abs/2303.08774>. arXiv:2303.08774 [cs].
- [6] D. Driess, F. Xia, M. S. M. Sajjadi, C. Lynch, A. Chowdhery, B. Ichter, A. Wahid, J. Tompson, Q. Vuong, T. Yu, W. Huang, Y. Chebotar, P. Sermanet, D. Duckworth, S. Levine, V. Vanhoucke, K. Hausman, M. Toussaint, K. Greff, A. Zeng, I. Mordatch, and P. Florence. PaLM-E: An Embodied Multimodal Language Model, Mar. 2023. URL <http://arxiv.org/abs/2303.03378>. arXiv:2303.03378 [cs].
- [7] V. S. Dorbala, J. F. Mullen, and D. Manocha. Can an Embodied Agent Find Your “Cat-shaped Mug”? LLM-Based Zero-Shot Object Navigation. *IEEE Robotics and Automation Letters*, 9(5):4083–4090, May 2024. ISSN 2377-3766. doi:10.1109/LRA.2023.3346800. URL <https://ieeexplore.ieee.org/document/10373065>. Conference Name: IEEE Robotics and Automation Letters.
- [8] A. Brohan, N. Brown, J. Carbajal, Y. Chebotar, X. Chen, K. Choromanski, T. Ding, D. Driess, A. Dubey, C. Finn, P. Florence, C. Fu, M. G. Arenas, K. Gopalakrishnan, K. Han, K. Hausman, A. Herzog, J. Hsu, B. Ichter, A. Irpan, N. Joshi, R. Julian, D. Kalashnikov, Y. Kuang, I. Leal, L. Lee, T.-W. E. Lee, S. Levine, Y. Lu, H. Michalewski, I. Mordatch, K. Pertsch, K. Rao, K. Reymann, M. Ryoo, G. Salazar, P. Sanketi, P. Sermanet, J. Singh, A. Singh, R. Soricut, H. Tran, V. Vanhoucke, Q. Vuong, A. Wahid, S. Welker, P. Wohlhart, J. Wu, F. Xia, T. Xiao, P. Xu, S. Xu, T. Yu, and B. Zitkovich. RT-2: Vision-Language-Action Models Transfer Web Knowledge to Robotic Control, July 2023. URL <http://arxiv.org/abs/2307.15818>. arXiv:2307.15818 [cs].
- [9] D. Shah, B. Osinski, B. Ichter, and S. Levine. LM-Nav: Robotic Navigation with Large Pre-Trained Models of Language, Vision, and Action. In *Proceedings of The 6th Conference on Robot Learning*, pages 492–504. PMLR, Mar. 2023. URL <https://proceedings.mlr.press/v205/shah23b.html>. ISSN: 2640-3498.
- [10] J. Ni and S. X. Yang. Bioinspired Neural Network for Real-Time Cooperative Hunting by Multirobots in Unknown Environments. *IEEE Transactions on Neural Networks*, 22(12):2062–2077, Dec. 2011. ISSN 1941-0093. doi:10.1109/TNN.2011.2169808. URL https://ieeexplore.ieee.org/abstract/document/6060919?casa_token=0BzAmcnZeKAAAAAA:W8_-gpjhr5KRlqNbwfk4S0kwK-v002YCxxwUNCBD1RpT17pNxDc9IF-NgQyTzImKV1RjFdlh. Conference Name: IEEE Transactions on Neural Networks.
- [11] Y. F. Chen, M. Liu, M. Everett, and J. P. How. Decentralized non-communicating multiagent collision avoidance with deep reinforcement learning. In *2017 IEEE International Conference on Robotics and Automation (ICRA)*, pages 285–292, May 2017. doi:10.1109/ICRA.2017.7989037. URL https://ieeexplore.ieee.org/abstract/document/7989037?casa_token=RStkd0_0xqIAAAAA:aiuK0Z45U5RxHqXdJBpCizCV4U9acJI1Jtw9uajpTqCnnPedB2j408iN4rnPA-xJv6GTr2_Z.
- [12] J. Blumenkamp, S. Morad, J. Gielis, Q. Li, and A. Prorok. A Framework for Real-World Multi-Robot Systems Running Decentralized GNN-Based Policies. In *2022 International Conference*

- on *Robotics and Automation (ICRA)*, pages 8772–8778, 2022. doi:10.1109/ICRA46639.2022.9811744.
- [13] C. Lynch, A. Wahid, J. Tompson, T. Ding, J. Betker, R. Baruch, T. Armstrong, and P. Florence. Interactive Language: Talking to Robots in Real Time. *IEEE Robotics and Automation Letters*, pages 1–8, 2023. ISSN 2377-3766. doi:10.1109/LRA.2023.3295255. URL <https://ieeexplore.ieee.org/document/10182264>. Conference Name: IEEE Robotics and Automation Letters.
- [14] B. Ichter, A. Brohan, Y. Chebotar, C. Finn, K. Hausman, A. Herzog, D. Ho, J. Ibarz, A. Irpan, E. Jang, R. Julian, D. Kalashnikov, S. Levine, Y. Lu, C. Parada, K. Rao, P. Sermanet, A. T. Tshen, V. Vanhoucke, F. Xia, T. Xiao, P. Xu, M. Yan, N. Brown, M. Ahn, O. Cortes, N. Sievers, C. Tan, S. Xu, D. Reyes, J. Rettinghouse, J. Quiambao, P. Pastor, L. Luu, K.-H. Lee, Y. Kuang, S. Jesmonth, N. J. Joshi, K. Jeffrey, R. J. Ruano, J. Hsu, K. Gopalakrishnan, B. David, A. Zeng, and C. K. Fu. Do As I Can, Not As I Say: Grounding Language in Robotic Affordances. In *Proceedings of The 6th Conference on Robot Learning*, pages 287–318. PMLR, Mar. 2023. URL <https://proceedings.mlr.press/v205/ichter23a.html>. ISSN: 2640-3498.
- [15] DFRobot. NVIDIA Jetson AGX Orin Large Language Model LLaMA2-7b and LLaMA2-13b Performance Test Report, 2023. URL <https://www.dfrobot.com>.
- [16] S. S. Kannan, V. L. N. Venkatesh, and B.-C. Min. SMART-LLM: Smart Multi-Agent Robot Task Planning using Large Language Models, Mar. 2024. URL <http://arxiv.org/abs/2309.10062>. arXiv:2309.10062 [cs].
- [17] Z. Mandi, S. Jain, and S. Song. RoCo: Dialectic Multi-Robot Collaboration with Large Language Models, July 2023. URL <http://arxiv.org/abs/2307.04738>. arXiv:2307.04738 [cs].
- [18] C.-M. Chan, W. Chen, Y. Su, J. Yu, W. Xue, S. Zhang, J. Fu, and Z. Liu. ChatEval: Towards Better LLM-based Evaluators through Multi-Agent Debate. Oct. 2023. URL <https://openreview.net/forum?id=FQepisCUWu>.
- [19] H. Zhang, W. Du, J. Shan, Q. Zhou, Y. Du, J. B. Tenenbaum, T. Shu, and C. Gan. Building Cooperative Embodied Agents Modularly with Large Language Models. Oct. 2023. URL <https://openreview.net/forum?id=EnXJfQy0K>.
- [20] K. Garg, J. Arkin, S. Zhang, N. Roy, and C. Fan. Large Language Models to the Rescue: Deadlock Resolution in Multi-Robot Systems, Apr. 2024. URL <http://arxiv.org/abs/2404.06413>. arXiv:2404.06413 [cs, math].
- [21] N. Reimers and I. Gurevych. Sentence-BERT: Sentence Embeddings using Siamese BERT-Networks. In *Proceedings of the 2019 Conference on Empirical Methods in Natural Language Processing*. Association for Computational Linguistics, Nov. 2019. URL <https://arxiv.org/abs/1908.10084>.
- [22] Z. Li, X. Zhang, Y. Zhang, D. Long, P. Xie, and M. Zhang. Towards General Text Embeddings with Multi-stage Contrastive Learning, Aug. 2023. URL <http://arxiv.org/abs/2308.03281>. arXiv:2308.03281 [cs].
- [23] C. Lee, R. Roy, M. Xu, J. Raiman, M. Shoeybi, B. Catanzaro, and W. Ping. NV-Embed: Improved Techniques for Training LLMs as Generalist Embedding Models, May 2024. URL <http://arxiv.org/abs/2405.17428>. arXiv:2405.17428 [cs].
- [24] R. S. Sutton and A. G. Barto. *Reinforcement learning: An introduction*. MIT press, 2018.
- [25] Y. Yang and J. Wang. An Overview of Multi-Agent Reinforcement Learning from Game Theoretical Perspective, Mar. 2021. URL <http://arxiv.org/abs/2011.00583>. arXiv:2011.00583 [cs].

- [26] R. Lowe, Y. Wu, A. Tamar, J. Harb, P. Abbeel, and I. Mordatch. Multi-agent actor-critic for mixed cooperative-competitive environments. In *Advances in Neural Information Processing Systems*, volume 2017-Decem, 2017. ISSN: 10495258.
- [27] T. Rashid, M. Samvelyan, C. S. d. Witt, G. Farquhar, J. Foerster, and S. Whiteson. Monotonic Value Function Factorisation for Deep Multi-Agent Reinforcement Learning. *Journal of Machine Learning Research*, 21(178):1–51, 2020. ISSN 1533-7928. URL <http://jmlr.org/papers/v21/20-081.html>.
- [28] J. Foerster, G. Farquhar, T. Afouras, N. Nardelli, and S. Whiteson. Counterfactual Multi-Agent Policy Gradients. *Proceedings of the AAAI Conference on Artificial Intelligence*, 32(1), Apr. 2018. ISSN 2374-3468. doi:10.1609/aaai.v32i1.11794. URL <https://ojs.aaai.org/index.php/AAAI/article/view/11794>. Number: 1.
- [29] C. S. de Witt, T. Gupta, D. Makoviichuk, V. Makoviychuk, P. H. S. Torr, M. Sun, and S. Whiteson. Is Independent Learning All You Need in the StarCraft Multi-Agent Challenge?, Nov. 2020. URL <http://arxiv.org/abs/2011.09533>. arXiv:2011.09533 [cs].
- [30] M. Tan. Multi-agent reinforcement learning: Independent vs. cooperative agents. In *Proceedings of the tenth international conference on machine learning*, pages 330–337, 1993.
- [31] L. Pan, T. Rashid, B. Peng, L. Huang, and S. Whiteson. Regularized Softmax Deep Multi-Agent Q-Learning. In *Advances in Neural Information Processing Systems*, volume 34, pages 1365–1377. Curran Associates, Inc., 2021. URL <https://proceedings.neurips.cc/paper/2021/hash/0a113ef6b61820daa5611c870ed8d5ee-Abstract.html>.
- [32] A. Kumar, A. Zhou, G. Tucker, and S. Levine. Conservative Q-Learning for Offline Reinforcement Learning. In *Advances in Neural Information Processing Systems*, volume 33, pages 1179–1191. Curran Associates, Inc., 2020. URL <https://proceedings.neurips.cc/paper/2020/hash/0d2b2061826a5df3221116a5085a6052-Abstract.html>.
- [33] A. Kumar, J. Fu, M. Soh, G. Tucker, and S. Levine. Stabilizing Off-Policy Q-Learning via Bootstrapping Error Reduction. In *Advances in Neural Information Processing Systems*, volume 32. Curran Associates, Inc., 2019. URL https://proceedings.neurips.cc/paper_files/paper/2019/hash/c2073ffa77b5357a498057413bb09d3a-Abstract.html.
- [34] J. Shao, Y. Qu, C. Chen, H. Zhang, and X. Ji. Counterfactual Conservative Q Learning for Offline Multi-agent Reinforcement Learning. *Advances in Neural Information Processing Systems*, 36:77290–77312, Dec. 2023. URL https://proceedings.neurips.cc/paper_files/paper/2023/hash/f3f2ff9579ba6deeb89caa2fe1f0b99c-Abstract-Conference.html.
- [35] S. Fujimoto and S. S. Gu. A Minimalist Approach to Offline Reinforcement Learning. In *Advances in Neural Information Processing Systems*, volume 34, pages 20132–20145. Curran Associates, Inc., 2021. URL https://proceedings.neurips.cc/paper_files/paper/2021/hash/a8166da05c5a094f7dc03724b41886e5-Abstract.html.
- [36] P. J. Ball, L. Smith, I. Kostrikov, and S. Levine. Efficient Online Reinforcement Learning with Offline Data. In *Proceedings of the 40th International Conference on Machine Learning*, pages 1577–1594. PMLR, July 2023. URL <https://proceedings.mlr.press/v202/ball123a.html>. ISSN: 2640-3498.
- [37] Y. Yang, X. Ma, C. Li, Z. Zheng, Q. Zhang, G. Huang, J. Yang, and Q. Zhao. Believe What You See: Implicit Constraint Approach for Offline Multi-Agent Reinforcement Learning. In *Advances in Neural Information Processing Systems*, volume 34, pages 10299–10312. Curran Associates, Inc., 2021. URL <https://proceedings.neurips.cc/paper/2021/hash/550a141f12de6341fba65b0ad0433500-Abstract.html>.

- [38] M. Liu, M. Zhu, and W. Zhang. Goal-Conditioned Reinforcement Learning: Problems and Solutions. In *Proceedings of the Thirty-First International Joint Conference on Artificial Intelligence*, pages 5502–5511, Vienna, Austria, July 2022. International Joint Conferences on Artificial Intelligence Organization. ISBN 978-1-956792-00-3. doi:10.24963/ijcai.2022/770. URL <https://www.ijcai.org/proceedings/2022/770>.
- [39] Y. Teh, V. Bapst, W. M. Czarnecki, J. Quan, J. Kirkpatrick, R. Hadsell, N. Heess, and R. Pascanu. Distral: Robust multitask reinforcement learning. In *Advances in Neural Information Processing Systems*, volume 30. Curran Associates, Inc., 2017. URL https://proceedings.neurips.cc/paper_files/paper/2017/hash/0abdc563a06105aee3c6136871c9f4d1-Abstract.html.
- [40] T. Schaul, D. Horgan, K. Gregor, and D. Silver. Universal Value Function Approximators. In *Proceedings of the 32nd International Conference on Machine Learning*, pages 1312–1320. PMLR, June 2015. URL <https://proceedings.mlr.press/v37/schaul15.html>. ISSN: 1938-7228.
- [41] J. Blumenkamp, A. Shankar, M. Bettini, J. Bird, and A. Prorok. The Cambridge RoboMaster: An Agile Multi-Robot Research Platform, May 2024. URL <http://arxiv.org/abs/2405.02198>. arXiv:2405.02198 [cs, eess].
- [42] M. Bettini, R. Kortvelesy, J. Blumenkamp, and A. Prorok. VMAS: A Vectorized Multi-Agent Simulator for Collective Robot Learning. *The 16th International Symposium on Distributed Autonomous Robotic Systems*, 2022. Publisher: Springer.
- [43] H. van Seijen, H. van Hasselt, S. Whiteson, and M. Wiering. A theoretical and empirical analysis of Expected Sarsa. In *2009 IEEE Symposium on Adaptive Dynamic Programming and Reinforcement Learning*, pages 177–184, Mar. 2009. doi:10.1109/ADPRL.2009.4927542. URL <https://ieeexplore.ieee.org/abstract/document/4927542>. ISSN: 2325-1867.
- [44] S. Emmons, B. Eysenbach, I. Kostrikov, and S. Levine. RvS: What is Essential for Offline RL via Supervised Learning? Oct. 2021. URL <https://openreview.net/forum?id=S874XAIpkR->.
- [45] J. L. Ba, J. R. Kiros, and G. E. Hinton. Layer Normalization. July 2016. URL <https://arxiv.org/abs/1607.06450>. eprint: 1607.06450.
- [46] B. Xu, N. Wang, T. Chen, and M. Li. Empirical evaluation of rectified activations in convolutional network. *arXiv preprint arXiv:1505.00853*, 2015.
- [47] Z. Wang, T. Schaul, M. Hessel, H. Hasselt, M. Lanctot, and N. Freitas. Dueling Network Architectures for Deep Reinforcement Learning. In *Proceedings of The 33rd International Conference on Machine Learning*, pages 1995–2003. PMLR, June 2016. URL <https://proceedings.mlr.press/v48/wangf16.html>. ISSN: 1938-7228.
- [48] S. Fujimoto, H. Hoof, and D. Meger. Addressing Function Approximation Error in Actor-Critic Methods. In *Proceedings of the 35th International Conference on Machine Learning*, pages 1587–1596. PMLR, July 2018. URL <https://proceedings.mlr.press/v80/fujimoto18a.html>. ISSN: 2640-3498.
- [49] X. Li and J. Li. Angle-optimized Text Embeddings. *arXiv preprint arXiv:2309.12871*, 2023.
- [50] F. Feng, Y. Yang, D. Cer, N. Arivazhagan, and W. Wang. Language-agnostic BERT Sentence Embedding. In S. Muresan, P. Nakov, and A. Villavicencio, editors, *Proceedings of the 60th Annual Meeting of the Association for Computational Linguistics (Volume 1: Long Papers)*, pages 878–891, Dublin, Ireland, May 2022. Association for Computational Linguistics. doi:10.18653/v1/2022.acl-long.62. URL <https://aclanthology.org/2022.acl-long.62>.

- [51] N. Muennighoff, N. Tazi, L. Magne, and N. Reimers. MTEB: Massive Text Embedding Benchmark. In A. Vlachos and I. Augenstein, editors, *Proceedings of the 17th Conference of the European Chapter of the Association for Computational Linguistics*, pages 2014–2037, Dubrovnik, Croatia, May 2023. Association for Computational Linguistics. doi:10.18653/v1/2023.eacl-main.148. URL <https://aclanthology.org/2023.eacl-main.148>.
- [52] S. Lee, A. Shakir, D. Koenig, and J. Lipp. Open Source Strikes Bread - New Fluffy Embeddings Model, 2024. URL <https://www.mixedbread.ai/blog/mxbai-embed-large-v1>.
- [53] L. Wang, N. Yang, X. Huang, L. Yang, R. Majumder, and F. Wei. Improving Text Embeddings with Large Language Models, Jan. 2024. URL <http://arxiv.org/abs/2401.00368>. arXiv:2401.00368 [cs].
- [54] S. Levine, A. Kumar, G. Tucker, and J. Fu. Offline Reinforcement Learning: Tutorial, Review, and Perspectives on Open Problems, Nov. 2020. URL <http://arxiv.org/abs/2005.01643>. arXiv:2005.01643 [cs, stat].
- [55] A. Shankar, S. Elbaum, and C. Detweiler. Freyja: A full multicopter system for agile & precise outdoor flights. In *2021 IEEE International Conference on Robotics and Automation (ICRA)*, pages 217–223. IEEE, 2021.
- [56] T. P. Lillicrap, J. J. Hunt, A. Pritzel, N. Heess, T. Erez, Y. Tassa, D. Silver, and D. Wierstra. Continuous control with deep reinforcement learning. In Y. Bengio and Y. LeCun, editors, *4th International Conference on Learning Representations, ICLR 2016, San Juan, Puerto Rico, May 2-4, 2016, Conference Track Proceedings*, 2016. URL <http://arxiv.org/abs/1509.02971>.

A SARSA and Expected SARSA

SARSA [24] is an on-policy method that learns the following Q function

$$Q_{\pi}(s, a) = R(s, a, s') + \gamma Q_{\pi}(s', a'), \quad (11)$$

where a' is the recorded action that taken in the environment. Notice the difference compared to standard Max Q learning, which utilizes a max operator and potentially out-of-distribution action a'

$$Q(s, a) = R(s, a, s') + \gamma \max_{a' \in A} Q(s', a'). \quad (12)$$

While Max Q learns the Q function for an optimal policy, SARSA learns a Q function for the policy that generated a' . Given these considerations, *SARSA is not expected to converge to an optimal policy* like Max Q is. Only as π approaches $\max_{a' \in A} Q_*(s, a)$ does expected SARSA approach the optimal policy. Although counter-intuitive, [24] shows how this suboptimal policy can be beneficial in the cliff walking scenario. In this scenario, the Max Q policy learns an optimal, but dangerous policy walking near the edge of a cliff to more quickly arrive at the goal. On the other hand, SARSA learns a safer policy that moves away from the cliff at the expense of a slightly reduced return. Even though Max Q should perform better in theory, in practice the Q function is imperfect and Max Q performs worse than SARSA [24].

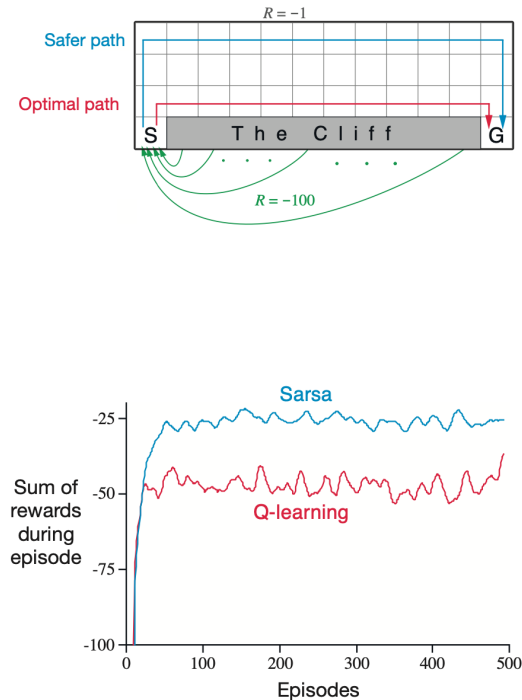


Figure 6: SARSA compared with Max Q, as it appears in [24]. SARSA learns a safer policy than Max Q on the cliff walking scenario. Max Q learns an optimal policy that remains close to the cliff edge, but reaches the goal more quickly. A single mistake can send the Max Q policy over the edge. In this case, SARSA samples uniform actions with probability 0.1 and behaves greedily otherwise, making it beneficial to create a gap between the agent and the edge. This results in a safer but less optimal policy. Even though Max Q should produce more optimal policies in theory, SARSA can outperform Max Q in practice.

While the SARSA update utilizes actions a' from the dataset, Expected SARSA uses the policy action distribution instead

$$Q_{\pi}(s, a) = R(s, a, s') + \gamma \sum_{a' \in A} \pi(a'|s) Q_{\pi}(s', a'). \quad (13)$$

A.1 Expected SARSA as a One Line Change to Q-Learning

In the text, we allude to a one-line code change to obtain expected SARSA from Max Q. Therefore, we demonstrate this change with some pseudocode. Here, q represents the Q function, g is the decay factor γ , s, a, r, sp correspond to the state, action, reward, and next state, d corresponds to the episode termination flag, and t corresponds to temperate τ . The difference between Max Q and Expected SARSA is how we compute `next_q.value`.

```
1 def max_q(q, g, s, a, r, sp, d):
2     q_value = q(s)[a]
3     next_q_value = q(sp).max()
4     target = r + !d * g * next_q
5     return q_value - target

1 def mean_q(q, g, s, a, r, sp, d):
2     q_value = q(s)[a]
3     next_q_value = q(sp).mean()
4     target = r + !d * g * next_q
5     return q_value - target

1 def soft_q(q, g, s, a, r, sp, d, t):
2     q_value = q(s)[a]
3     next_q_value = (softmax(q(sp) / t) * q(sp)).sum()
4     target = r + !d * g * next_q
5     return q_value - target
```

A.2 The Relationship Between Offline Expected SARSA and Importance Sampling

We can view the offline Expected SARSA formulation as similar to Importance Weighted Off-Policy SARSA [24, 7.3]. If we assume a uniform prior π_β , then the importance sampling weight is given by

$$\frac{\pi(s)}{\pi_\beta(s)} = \frac{\pi(s)}{1/|A|} = |A|\pi(s) \tag{14}$$

because

$$\pi_\beta(s) = \mathcal{U}(A), \pi_\beta(a|s) = \frac{1}{|A|} \quad \forall a, s. \tag{15}$$

Since $|A|$ is a constant, we can say that the Expected SARSA Q values are proportional to those learned by Off-Policy SARSA under importance sampling.

B Additional Experiments

We provide a number of additional experiments. We perform ablations on CQL and Soft Q hyperparameters, evaluate CQL and Max Q in the real world, and further inspect the results of our five-agent robot experiments. Finally, we briefly discuss a decentralized form of our method.

B.1 CQL and Soft Q Ablation Studies

To find ideal CQL regularization strengths α and soft Q temperatures τ , we perform an ablation in Fig. 7. We spawn the agents randomly in the arena, and sample random goals for each agent. We repeat this test five times every 1000 updates of the Q network.

B.2 Max Q and CQL in the Real-World

In this subsection, we provide results for the Max Q and CQL objectives in the real world. Similar to simulation, the agents learn to maximize the distance between themselves to avoid collisions, but never manage to learn to navigate to the provided goals (Fig. 8, Fig. 9).

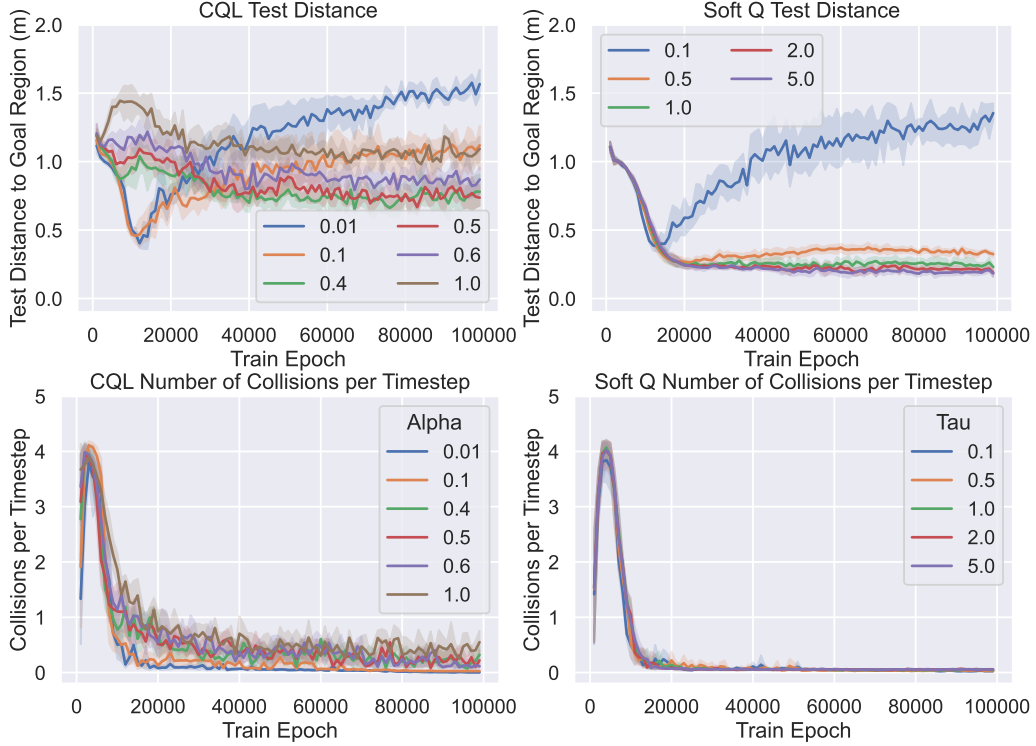


Figure 7: Comparing CQL and Expected SARSA soft Q losses in simulation. (Top) We consider CQL with a variety of regularization strengths α and Expected SARSA Soft Q with a number of temperatures τ . We inspect both the mean distance to the goal over an episode, as well as the number of collisions with the boundaries or other agents over an episode. Greater CQL regularization appears to reduce overextrapolation at the cost of a largely suboptimal policy. Expected SARSA Soft Q exhibits more stable training, resulting in more optimal policies with virtually no collisions. Note that as we decrease τ , the Soft Q objective approaches Max Q, and we observe overextrapolation for $\tau = 0.1$ and to a lesser extent $\tau = 0.5$

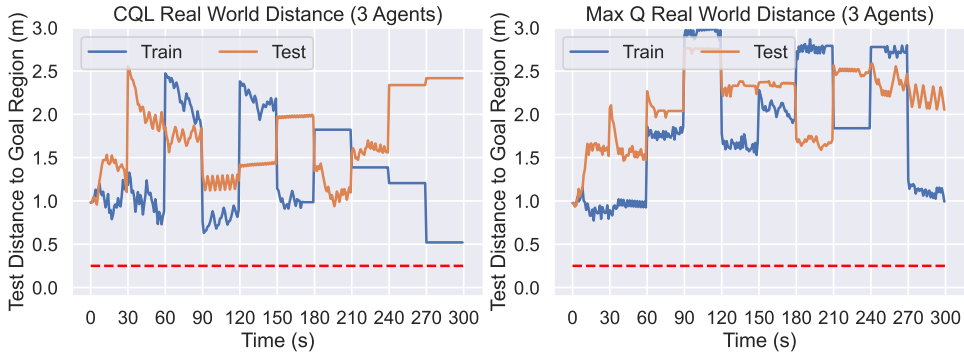


Figure 8: The real-world experiments for the CQL and Max Q objectives. We report the distance to goal, taking the mean across all agents. Neither method performs particularly well.

B.3 Investigating Real-World Collisions

Although we did not observe any collisions in the three-agent real-world scenarios, we observed two minor grazes (less than a second of contact on diagonal points) in the five-agent real-world experiments. Let us further investigate these collisions.

In our investigation, we visualise the positions of the robots, as logged by ROS and motion capture system in Fig. 10. Interestingly, we find that according to our raw logs, *no agents* ever collide even

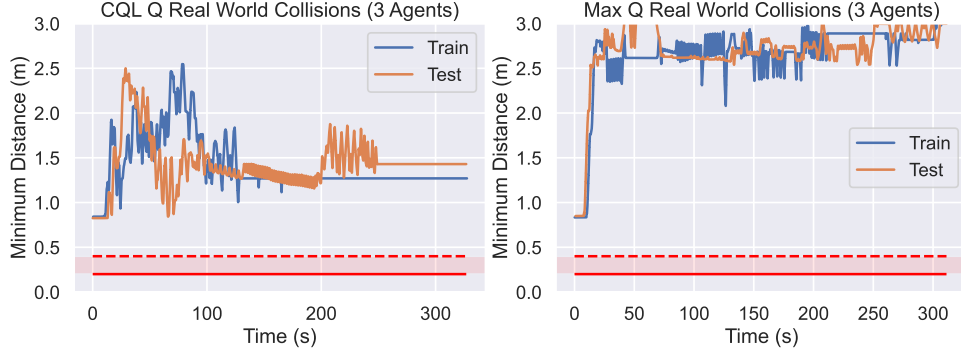


Figure 9: The real-world experiments for the CQL and Max Q objectives. We report the number of collisions, taking the mean across all agents. Both methods are capable of avoiding collisions and remaining within the boundaries. Any distances below the dotted red line are where agents breach their safety boundary of 40 cm, while the solid red line denotes a collision in the physical world.

though they might approach quite close to each other. The shaded red region in the figure indicates our collision thresholds, and we find that the minimum distance between all robots is always above the hard threshold (solid red).

We attribute this to small offsets in the rigid-body’s centroid (as tracked by motion capture) compared to the actual geometric pivot of the robots. This is primarily why the logs don’t show a collision. These offsets produce compounded effects since the robots have a rectangular base (i.e., the diagonal may appear artificially shifted), and thus the controller’s outputs can induce a slight twist on the body. Furthermore, in our ROS ecosystem, we run motion capture in a best-effort mode, and observe rare spikes in network latency due to congestion (especially when high-frequency logging is active). We note in Fig. 10 (bottom-right) that our policies do not generate actions that lead to obvious collisions: the two robots approach very close, but their actions are pointed in different directions. These close approaches may be avoided by increasing the distance threshold further.

B.4 Distributed Policies

Although we execute our policies in a centralized manner in our experiments, there also exists a decentralized equivalent. Using decentralized policies enables agents to compute and take actions on their own. Let us rewrite our embeddings z_i , states s_i , and actions a_i to make this clear

$$z_i = \phi(g_i) \tag{16}$$

$$s_i = f(o_i, z_i, o_{1:(i-1)}, (i+1):n, z_{1:(i-1)}, (i+1):n) \tag{17}$$

$$\pi(a|s_i) = \frac{e^{Q(s_i, a)/\tau}}{\sum_{\alpha \in A} e^{Q(s_i, \alpha)/\tau}} \tag{18}$$

$$a_i \sim \pi(a|s_i) \tag{19}$$

We see that each agent’s action a_i depends only on the observations o and latent tasks z of itself and the other agents. Once we have computed the state s_i , the policies can independently compute the action a_i . In other words, all computation (f, π) can be computed independently.

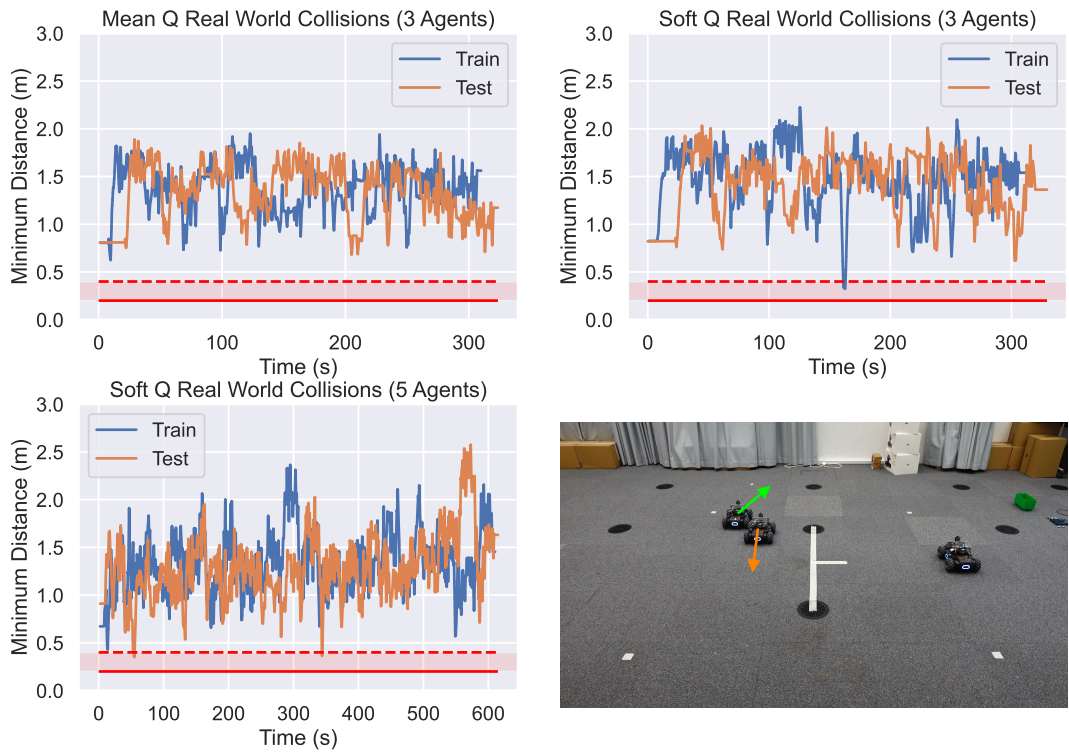


Figure 10: We plot the minimum distance observed between all robots, as reported by our motion capture system and recorded by ROS2. Any distances below the dotted red line are where agents breach their safety boundary of 40 cm, while the solid red line denotes a collision in the physical world. Although we observe two minor scrapes in the five-agent videos, our data suggests that no collisions occurred. The image on the bottom right corresponds to point in time with the lowest minimum distance for the three-agent Soft Q objective (around 160s). Even though the safety boundary is breached, there is no physical collision.

C Experiment Details

In this section, we provide further details for the LLM latent space experiment and the RL experiments.

C.1 LLM Latent Space Details

For the LLM decoder experiment Fig. 3, we utilize a $k = 1.1$ m and train using mean squared error. Our neural network consists of three blocks B (linear layer, layernorm, and leaky ReLU, see Section 4.2) followed by a final linear layer.

Hyperparameter	Value
Batch size	32
Learning rate	0.00001
Learning rate warmup epochs	0
Optimizer	Adamw
Weight decay	0.0001
$ z $	768
Hidden size	256

Table 1: Decoder hyperparameters for the LLM analysis experiment.

C.2 Real-World Experimental Setup and Framework

Here we provide additional details on the robots as well as the framework we use for all our experiments. The robotic platforms we use are DJI Robomaster S1 platforms, which are customized similar to prior work [41]. The robots have an omnidirectional mecanum-wheel drive, and can track fixed-frame position and velocity state references using an onboard control stack (*Freyja* [55]). The robots have a radius of approximately 25 cm. We operate within a 3.8 m \times 3.8 m subset of a larger 6 m \times 4 m motion-capture arena. We use the default North-East-Down frame convention (with the Down component always zero for ground robots), which is why some of the text prompts contain cardinal directions (‘north edge’) in them.

The actions generated by our trained policies are fixed-frame velocity targets for the robot, commanded at 1 Hz, and are tracked by the onboard controller at 50 Hz. Note that since our policies take < 2 ms to generate actions, we can potentially run them at substantially higher rates if necessary. However, with discretized actions, we find that an action frequency of 1 Hz is sufficient for the navigation tasks we consider. Our control stack, motion-capture setup and the policy execution are all wrapped in a ROS2 ecosystem, and the exact framework is also utilized for collecting real-world datasets.

C.3 RL Training Details

We list the hyperparameters used for both the simulated and real-world RL experiments in Table 2. We provide an arena to the agents, outside of which is considered a collision. During training, we approximate the collision radius of each agent as 0.4 m. During deployment, our actions come from a Boltzmann policy with a temperature of $\tau = 0.01$

$$\pi(a|s_i) = \frac{e^{Q(s,a)/\tau}}{\sum_{\alpha \in A} e^{Q(s,\alpha)/\tau}} \tag{20}$$

$$a_i \sim \pi(a|s_i). \tag{21}$$

Each agent i shares the same parameters for π . We update the Q function using a Polyak soft update [56].

Hyperparameter	Value
Decay γ	0.95
Polyak τ	0.0005
Batch size	256
Learning rate	0.0001
Learning rate warmup	linear
Learning rate warmup epochs	1000
Optimizer	Adamw
Weight decay	0.0001
$ z $	768
Hidden size	1024
LLM	GTE-Base
Ensemble size	2
Ensemble reduce	min
Simulation	
Evaluation episodes per epoch	5
Timesteps per evaluation episode	50
Collision radius	40 cm
Epochs trained	100k
Real World	
Evaluation episodes	10 or 20
Timesteps per evaluation episode	30
Epochs trained	1M
Collision radius	20 cm - 30 cm

Table 2: Hyperparameters shared between all RL experiments.

D Tasks

We provide a list of commands and locations that we use to generate tasks. All tasks are in the form Agent, <command to location>. We generate train commands by combining a location with a command string. The {} denote where the location goes in the command string.

	west edge
	east edge
	south edge
	north edge
	left edge
	right edge
	bottom edge
	top edge
	lower edge
	upper edge
	south west corner
	west south corner
	south east corner
	east south corner
	north west corner
	west north corner
	north east corner
	SW corner
	SE corner
	NW corner
	NE corner
	bottom left corner
	left bottom corner
	bottom right corner
	right bottom corner
	top left corner
	left top corner
	top right corner
	right top corner
	lower left corner
	left lower corner
	lower right corner
	right lower corner
	upper left corner
	left upper corner
	upper right corner
	right upper corner
navigate to the {}	
pathfind to the {}	
find your way to the {}	
move to the {}	
your goal is the {}	
make your way to the {}	
head towards the {}	
travel to the {}	
reach the {}	
proceed to the {}	
go to the {}	
the {} is your target	